Skeletonization of renal cysts of autosomal dominant polycystic kidney disease using magnetic resonance imaging

（MRI 画像を用いた ADPKD 腎領域に対する skeletonization アルゴリズムの適用）

千葉大学大学院医学薬学府

先端医学薬学専攻

（主任：市川　智彦　教授）

寺中　さやか

Abstract

Autosomal dominant polycystic kidney disease (ADPKD) is a condition in which numerous cysts develop in the renal tubules and grows over the lifetime, resulting in compression of renal parenchyma and worsens renal function. Conventionally, total kidney volume (TKV) is bluntly estimated as a time cross sectional parameter of disease status. In assumption that cyst initiation rate and growth speed of cysts would be another prognostic marker for renal function, and regulate the morphological feature of the enlarged kidney, we attempted to extract a morphological feature of the renal cystic region quantitatively from MRI T2-weighted images. Skeletonization algorithm was applied to the binarized cystic region after extracting cystic regions by discriminant analysis. Then, morphological feature of the renal cystic region was converted to distribution pattern in number and size of cysts, and "branch" of adjacent cysts. The number of "branches" corresponded with the number of cysts, and the cumulative probability curves of "branch" length shifted according to cyst size distribution. The proposed method successfully quantified morphological feature of cystic region objectively in semi-automatic manner. The method would contribute to manage ADPKD patients in deciding time to start therapies after affirmation for consistency with cyst initiation rate, growth speed of cysts and renal function.

Introduction

Autosomal dominant polycystic kidney disease (ADPKD) is a hereditary, progressive disorder that is characterized by a gradual increase of cysts and kidney volume with subsequent renal insufficiency[1,2]. The Consortium for Radiologic Imaging Studies of Polycystic Kidney Disease (CRISP) study has shown that total kidney volume (TKV) can predict the progression of increasing TKV and subsequent renal insufficiency[3]. However, the good correlation between TKV and the prognosis of this disease is confined to only when kidney enlargement advances obviously[4].

While many patients with ADPKD require hemodialysis by the fifth to seventh decade of life, some patients do not develop renal insufficiency in their lifetime[5]. There are substantial individual differences in the long-term progression of the disease[3,4] that also make a prediction of the likelihood of renal insufficiency in the early stage difficult, and should be solved to reduce burden of therapies in both physical and economical aspects[6].

In the early stage of the disease, the renal cysts are considered to develop and enlarge without the increasing of TKV. In the previous report, a growth speed of cysts was indicated to be a factor responsible for increase of TKV[7]. In contrast, another report revealed that growth speed of cysts was rather uniform, and earlier initiation of cysts was potent prognostic factor for developing renal insufficiency in relation to cytogenetical findings[8]. However, the methods to estimate such prognostic factors are limited to cytogenetical investigation or use of mathematical models that require manual counting of numerous cysts[7,8]. It could be assumed that multifocal and constant sprout of cyst would

determine morphological appearance of the kidney afterward, the affinity of cyst initiation in renal tubules would be diagnosed by analyzing temporal images of the enlarged kidney, especially using magnetic resonance (MR) T2-weighed imaging. Since the most cysts are agglutinated and their boundary are often unclear, shape, number of each cyst and agglutinated condition should be converted to numerical parameter before analysis. The skeletonization algorithm is used to convert shapes into a group of lines for computational recognition and tracking of objects[9,10], and the morphological analysis using a thinning and skeletonization algorithm has been widely used for medical applications[11]-[18].

The purpose of this study is to develop a software program that contains a semi-automatic binarization of renal cyst regions in an MRI T2 image and a skeletonization algorithm, and validated acquired numerical parameters using cyst-like geometrical models and MR images of patients with ADPKD.

Materials and Methods

The MRI were performed as routine clinical practice using MAGNETOM Symphony (Siemens, Erlangen, Germany), and the images were provided for this study under approval by the local ethics committee of Chiba East Hospital and Chiba University Hospital. The imaging protocol was T2-weighted imaging (Half-Fourier single-shot turbo spin echo: HASTE), with coronal cross sections, slice thickness of 4 - 10 mm, and spatial resolution of 1.67 mm/pixel. One image for processing was selected from each image series containing the renal pedicle, and the pixel intensity was compressed into an 8-bit value range. The algorithm of image processing was as follows and is shown in Figs. 1 and 2.

The first step was image binarization of the cystic region. Since the intensity of cystic region varies widely and cause over and under extraction in the binarization process, a look up table (LUT) was applied as contrast enhancement for the mid-range values[19,20]. The LUT curve was generated using a sigmoid function as follows,

$$\varsigma(x) = \frac{256}{1+e^{-0.05(x-b)}} \qquad (1)$$

where $\varsigma(x)$ is the output value against the input intensity value x, and b is a value that determines the inflection point of the sigmoid curve. The adjustment of b is mentioned in the next section.

To determine a proper threshold value for cyst region extraction, outlines of both kidneys were pre-segmented manually by a urologist as two polygonal regions. Then a threshold value was determined to divide renal parenchyma and cyst into two classes using a discriminant analysis

according to Otsu's method.

In the second step, the morphological analysis was processed to the binarized cystic area to quantify the features of the cystic region, such as density and size distribution of the renal cysts. In this study, a skeletonization algorithm was applied to the binary image that would show the morphological characteristics of the cysts without recognizing and counting individual cysts.

Implementation

MR images for processing were reviewed, selected, and compressed into 8-bit TIFF format with an open source DICOM viewer OsiriX. The algorithm was implemented using MATLAB® 2014b (Mathworks, Inc., Natick, MA, USA). On the originally designed Graphical User Interface (GUI), the operator can select an option of wiener-filtering, the "wiener2" function in MATLAB®, as a noise-reducing pre-processing step. Besides, the user can manually change the value of *b* in equation (1) with a slider interface. The GUI showed the result of contrast enhancement and binarization images simultaneously so that the operator can find a proper value with iterative trials. The discriminant analysis and skeletonization method were applied using the built-in functions "graythresh" and "bwmorph (skel)" in MATLAB® and Image Processing Toolbox™, respectively. Finally, the software provided the skeletonized image of the renal cystic regions. The branch points were extracted using "bwmorph (branchpoint)" in MATLAB®, and then the points were eroded and subtracted from the skeletonized image to separate each branch. The length of each branch was

calculated using a labeling algorithm.

Basic evaluation with the cyst-like geometric model

To evaluate whether the branches acquired with the proposed algorithm substitutes the morphological features of the cystic region, the developed software was tested with the cyst-like geometric models that simulate various densities (number) and sizes of renal cysts in the polycystic kidney. The experimental data that assume a binarized cystic region were designed on a 256×256-pixel image. The relationship of cysts and branches were tested using two sets of test images. The first set consisted of 20 images with different numbers (n=10, 15, 20, 25, and 30) of uniform size of cysts (radius S:5, M:10, L:15, LL:20 pixels, respectively, Fig. 3). For another set of five images, a mixture of different sizes (M, L, LL) and a fixed number (n=30) of cysts were depicted in each image (Fig. 4). In Fig. 4, each image consists of (a) 20 M size and 10 L size, (b) 10 M size and 20 L size, (c) 10 M size, 10 L size, and 10 LL size, (d) 20 L size and 10 LL size, and (e) 10 L size and 20 LL size circles, respectively. Since each center of the circle was placed randomly, the circles are unintentionally merged that express the similar condition of the cystic regions in renal parenchyma.

With the former image set, the linearity between number of branches and cysts, and the stability of the value for the cyst size were tested. While the length and number of extracted branches from the latter group images were displayed as the cumulative density functions (CDF) to investigate the relationship between branch length distribution and different mixture property of cyst size.

Evaluation with MR images of ADPKD

The 18 MR images of 12 patients with ADPKD were used in the present study. The patients had been followed up at Chiba East Hospital from August 2009 to May 2015. Their age ranged from 42 to 67 years, and estimated Glomerular Filtration Rate ranged between 8.4 to 90.1 ml/min/1.73 m^2. The 18 series of T2-weighted coronal abdominal MR image set were processed with the proposed algorithm. To evaluate the processing accuracy, each cyst was manually traced by a urologist. The minimum countable cyst size of manual tracing was 1×1 pixel (approximately 1.9 mm^2). Then, the total cyst area and distribution of approximate radius of each renal cyst, that is derived using the area of each cyst, were utilized as the reference data.

First, the accuracy of the area of the extracted cystic region was calculated to evaluate the binarization process. Secondly, we evaluated whether the distribution of branch length translates the mixture property of the cystic size. The subjects were dichotomized by the number of cysts from the reference data. The larger number group tended to have numerous small cysts (Group A), while the other group consisted of scattered large cysts (Group B). The distribution of branch length of each subject was expressed as a CDF and the area under the curve (AUC) of the CDF[21] was compared between the two groups.

Results

Evaluation with the cyst-like geometric model

Fig. 3 revealed the results of skeletonization of the geometric cyst-like models that contained the same-sized circle. The dependency of the circle count on circle size was tested, and the branch tended to be depicted like a radius of each circle even if the circles contacted or overlaid each other. Since the skeletonization algorithm returned one branch point and four branches for each independent circle, the regression coefficient between the number of branches and circles will be four if all circles are isolated. As shown in Fig. 5, the numbers of branches were clearly correlated with the designed circle count (r=0.99, 0.99, 0.99 and 0.98, respectively from S to LL) and the regression coefficient (Coef) was comparable among M, L and LL (3.4, 2.7 and 2.0, respectively). On the other hand, the Coef of S size group stayed in a small rate of 1.3, indicating the presence of lower limit size to detect cyst properly.

Next, Fig. 6 shows the CDF of the lengths of branches in each processed image appeared in Fig. 4. With an increase in the ratio of small-sized circles, the curve increased earlier than the pattern, which is filled with uniformly large circles.

These two empirical observations showed that the count of branches should translate the number of the cysts (except for the very small cysts), and a number of the same length branch would correlate to a number of cysts with a radius same as the branch length. In addition, the CDF of branch length was also suggested to be useful to compare the mixture property of the cyst size.

Evaluation with MR images

The total area of the cysts of each image contoured by a urologist ranged from 85 to 330 cm² (median 153 cm²), while the total renal cyst area measured with the binarization process ranged from 96 to 341 cm² (median 181 cm²). These two values were strongly correlated (Fig.7, r=0.97) with a high Coef (0.99), however, the regression line also suggested 22.7 cm^2 of positive bias of the segmented area to the reference. The average error was 13.7 %. In addition, the geometrical model test has shown that the total number of the extracted branches for each subject was positively correlated with the cyst count (r =0.81, Coef = 0.73) even for the cystic region in a MR image which is an imperfect circular composition (Fig. 8).

Nine images included in the Group A had the significantly larger number of cysts and branches than the other group (Table 1). Fig.9 shows example images of both groups with skeletonization and Fig. 10A shows the CDF against the cyst area intervals of 4 samples illustrated in Fig. 9. The renal region contained many small cysts in Group A (shown as red lines) in this study; thus, the curve was shown in the upper area than the Group B (shown as blue lines). At the same time, in the CDF of the branch length (Fig. 10B), the pattern of distribution corresponded to the reference. In addition, the average curves of each group (Fig. 11) also revealed upward shift for group A for both reference and branch analysis. Furthermore, the average AUC of group A was significantly greater than that of group B with the reference data, and marginal significance was observed in the branch data (Table 1).

Discussion

The binarization process for MR image

In the present study, automatic extraction of cystic regions was still challenging. One reason was the intensity values of cysts overlap with those of renal blood vessels and liver cysts, which is a frequent complication in patients with ADPKD. As with the progress of the disease, kidneys often extended and had close contact with the liver. Since such conditions inhibit automated segmentation renal cysts, manual pre-segmentation of the renal region was required in the current software to separate the liver and kidney regions roughly. This process may be replaced with automated segmentation on the prior statistical information of kidney location[22] for the further application. In addition, the manual contrast adjustment was required in the present study. As shown in Fig. 7, the consistent region of the cyst was successfully extracted, though the procedure was subjective manner. Limitation of the study is "one-man handling" of all the images that lacks verification of reproducibility by several operators. However, our preliminary trials suggested the proper parameter (b) in the contrast enhancement has proper range, and the result quality was rather deteriorated with out of range values (data not shown). Thus, we expect such property can minimize the variability by the operator and would roughly ensure the reproducibility of the result. In addition, the constant error, +13.7 % to the actual area, was attributable to the under-segmentation of the reference data, because the agglutinated cyst must be counted separately and includes systematic error at the unit conversion. Therefore, the bias was expected not to affect the distribution pattern of the branch length.

The skeletonization algorithm

The branches, extracted as a morphological descriptor in cysts, should encompass linearity between a total number of cysts and branches without the dependency on the cyst size and the ratio of agglutination. The branches were grown to the diagonal direction and generally consisted of a fewer number of pixel than the Euclid distance. The geometric models' evaluation suggested the branches from S size (5-pixel radius) circles were undercounted comparing to the other larger circles. The branches with short Chebyshev distance were eliminated, because the dilated regions of each cross-point were used for isolating the connected branches. While, the process positively affected for the large cyst component to remove noisy branches. Our preliminary study observed the lower limit of proper branch extraction was a circle of six-pixel radius, which represents a cyst of about 15 mm in diameter for the MR images in this study. Since this limitation simply depends on the spatial resolution ability of the imaging modality, the imaging protocol optimization may improve the restriction. For example, the current development of MRI enabled visual detection of tiny cysts, with diameters of around 1 mm[23].

On the other hand, the data correlation of the geometrical data (using M, L and LL) showed Coef=2.7 and r=0.99 for M, L, and LL data, and Coef =2.3 and r=0.57 for the MR data after the exclusion of the data under limitation, respectively. The similarity of two regression coefficient also suggested the dependency of number of branch lines on both the cyst size and the agglutinated ratio.

For these reasons, the distribution of branch length may under-evaluate the mixture rate of small cyst

and is discussed further in a following section.

Effect of CDF & AUC

The CDF of the branch length was used to show the mixture pattern of cyst size and compare them among the different TKV. As shown in Fig. 11, the CDF curve of the branch lines has implied a method to identify the mixture pattern of the cyst size as well as the manually counted data. Though the difference between the curves was not statistically significant, it is attributable to small sample size and separation method using the median value of number of cysts. Besides, differences between groups become rather small at the short branch length region. That might be resulted from the miscounting error of branches in tiny cysts. Thus, the improvement of algorithm to count the short branches consistently would show the difference more clearly between the different cyst growth patterns.

These results would afford us to consider that the CDF comparison would be an indicator to track the chronological behavior of the cysts. In patients with high cyst initiation rate, the CDF curve would shift to the left, and in the case of rapid growth speed of cyst, the CDF curve would shift to the right. Cyst growth parameters such as cyst initiation rate and growth speed would not change over a lifetime[8]. Though changes of cysts on MR images over subsequent years are generally small and difficult to recognize visually, we expect that the CDF pattern would be potent to quantify cyst growth parameters combined with the statistical analysis[24]. Besides, CDF pattern describe personalized

character of cysts' growth without manually counting and would add prognostic information at TKV measurement.

Further studies were required to track and analyze the chronological CDF changes in various progression pattern of ADPKD using prospective protocol and/or animals.

Conclusion

A skeletonization algorithm was applied to renal MR images in patients with ADPKD. Distribution of branch length showed a mixed style of cyst size without tracing each cyst and would enable detection of morphological and chronological changes of renal cysts to help prediction of the prognosis of renal function in these patients.

References

1. V. E. Torres, P. C. Harris, and Y. Pirson, Autosomal dominant polycystic kidney disease, Lancet. 369, 1287–1301 **(2007).**

2. P. D. Wilson, Polycystic Kidney Disease, N. Engl. J. Med. 350, 151–164 **(2004)**.

3. J. J. Grantham, A. B. Chapman, and V. E. Torres, Volume progression in autosomal dominant polycystic kidney disease: the major factor determining clinical outcomes, Clin. J. Am. Soc. Nephrol. 1, 148–157 **(2006)**.

4. K. T. Bae, P. K. Commean, and J. Lee, Volumetric measurement of renal cysts and parenchyma using MRI: phantoms and patients with polycystic kidney disease, J. Comput. Assist. Tomogr. 24, 614–619 **(2000).**

5. P. Ruggenenti, F. Gaspari, A. Cannata, F. Carrara, C. Cella, S. Ferrari, N. Stucchi, S. Prandini, B. Ene-Iordache, O. Diadei, N. Perico, P. Ondei, A. Pisani, E. Buongiorno, P. Messa, M. Dugo, and G. Remuzzi, Safety and efficacy of long-acting somatostatin treatment in autosomal-dominant polycystic kidney disease, Kidney Int. 68, 206–216 **(2005).**

6. M.Parramon, R.Peces, C.Peces, and R. Selgas, Economic Burden Of Adpkd From The Spanish Health System And Patient's Perspective: Advantages Of Delaying Dialysis, Value Health 18**,** A509 **(2015)**.

7. J. J. Grantham, L. T. Cook, V. E. Torres, J. E. Bost, A. B. Chapman, P. C. Harris, L. M. Guay-Woodford, and K. T. Bae, Determinants of renal volume in autosomal-dominant polycystic kidney disease, Kidney Int. 73, 108–116 **(2008)**.

8. P. C. Harris, K. T. Bae, S. Rossetti, V. E. Torres, J. J. Grantham, A. B. Chanpman, L. M. Guay-Woodford, B. F. King, L. H. Wetzel, D. A. Baumgarten, P. J. Kenney, M. Consugar, S. Klahr, W. M. Bennett, C. M. Meyers, Q. J. Zhang, P. A. Thompson, F. Zhu, and J. P. Miller, Cyst number but not the rate of cystic growth is associated with the mutated gene in autosomal dominant polycystic kidney disease, J. Am. Soc. Nephrol. 17, 3013–3019 **(2006).**

9. H. Fujiyoshi, and A. J. Lipton, Real-time human motion analysis by image skeletonization.Proceedings of Fourth IEEE Workshop on Applications of Computer Vision, **(1998)** October 15-21; Princeton, NJ, USA.

10. M. Naf, O. Kubler, R. Kikinis, M. E. Shenton, and G. Szekely, Characterization and recognition of 3D organ shape in medical image analysis using skeletonization. Proceedings of the Workshop on Mathematical Methods in Biomedical Image Analysis, **(1996)** June 21-22; San Francisco, CA, USA

11. K. Palágyi, E. Balogh, A. Kuba, C. Halmai, B. Erdőhelyi, E. Sorantin, and K. Hausegger, A Sequential 3D Thinning Algorithm and Its Medical Applications. Proceedings of the 17th International Conference on Information Processing in Medical Imaging, **(2001)** June 18-22; Davis, CA, USA

12. Y. Chen, K. Drechsler, W. Zhao, and C. O. Laura, A Thinning-based Liver Vessel Skeletonization Method. Proceedings of 2011 International Conference on Internet Computing and Information Services, **(2011)** September 17-18; Hong Kong,China

13. S. Y. Wan, A. P. Kiraly, E. L. Ritman, and W. E. Higgins, Extraction of the hepatic vasculature in rats using 3-D micro-CT images, IEEE Trans. Med. Imaging 19, 964–971 **(2000).**

14. N. Niki, K. Kanazawa, H. Satoh, H. Ohmatsu, and N. Moriyama, Computer assisted diagnosis of lung cancer using helical X-ray CT. 1994 IEEE Conference Record of Nuclear Science Symposium and Medical Imaging Conference, **(1994)** October 30-November 5; Norfolk, VA, USA

15. K. Kanazawa, N. Niki, H. Satoh, H. Ohmatsu, and N. Moriyama, Computer assisted diagnosis of lung cancer using helical X-ray CT. Proceedings of IEEE Workshop on Biomedical Image Analysis, **(1994)** June 24-25; Seattle, WA, USA

16. S. F. Huang, R. Chang, Analysis of tumor vascularity using three-dimensional power Doppler ultrasound images, IEEE Trans. Med. Imaging 27, 320–330 **(2008)**

17. Q. Ji, J. Engel, and E. Craine, Texture analysis for classification of cervix lesions, IEEE Trans. Med. Imaging 19, 1144–1149 **(2000).**

18. A. Nedzved, S. Ablameyko, and I. Pitas, Morphological segmentation of histology cell images. Proceedings of 15th International Conference on Pattern Recognition, **(2000)** September 3-7; Barcelona, Spain

19. G. J. Braun , M. D. Fairchild, Image lightness rescaling using sigmoidal contrast enhancement functions, J. Electron. Imaging. 8**,** 380–393 **(1999).**

20. A. F. Laine, S. Schuler, J. Fan, and W. Huda, Mammographic Feature Enhancement by

Multiscale Analysis, IEEE Trans. Med. Imaging. 13, 725–740, **(1994).**

21. R.García, New Insights on Multidimensional Image and Tensor Field Segmentation, Presses university de Louvain, Belgium**(2007).**

22. K. Bae , B. Park , H. Sun , J .Wang , C. Tao , A.B. Chapman , V.E. Torres, J.J. Grantham, M. Mrug, W.M. Bennett , M.F. Flessner, DP Landsittel,and K.T. Bae, Segmentation of individual renal cysts from MR images in patients with autosomal dominant polycystic kidney disease. Clin. J. Am. Soc. Nephrol. 8, 1089–1097 **(2013).**

23. J. J. Grantham, S. Mulamalla, C. J. Grantham, D. P. Wallance, L. T. Cook, L. H. Wetzel, T. A. Fields, and K. T. Bae, Detected renal cysts are tips of the iceberg in adults with ADPKD, Clin. J. Am. Soc. Nephrol. 7, 1087–1093 **(2012).**

24. T.Yamaguchi, and H. Hachiya, Proposal of a parametric imaging method for quantitative diagnosis of liver fibrosis, J. Med. Ultrason. 37, 155–66 **(2010)**.

Figure 1. The image processing algorithm

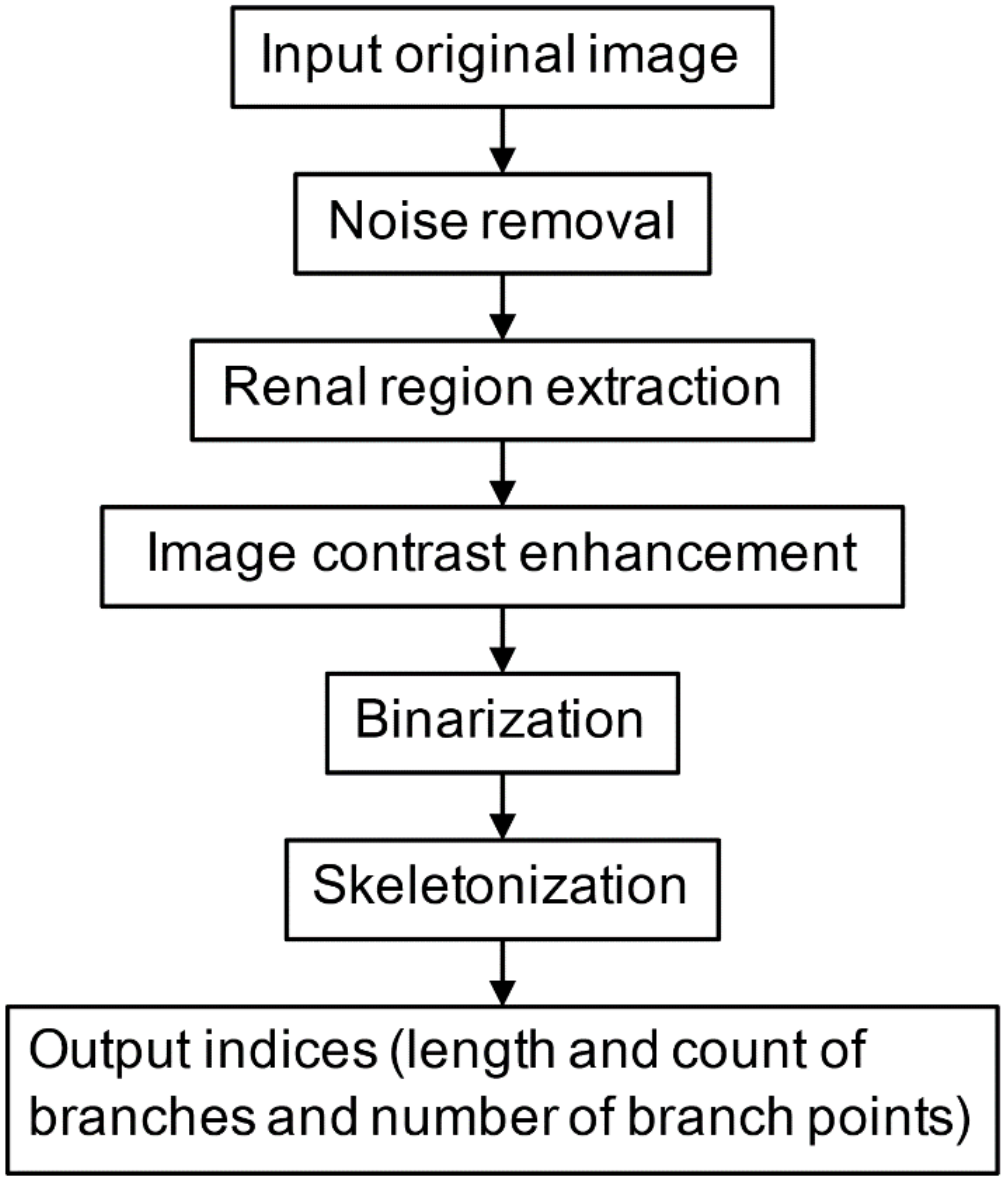

Figure 2. Steps of skeletonization(A) Original MR image, (B) Renal cystic region obtained by binarization, (C) Extracted branches, (D) Magnified part of (C). Orange lines are branches, and branch points are depicted as green dots.

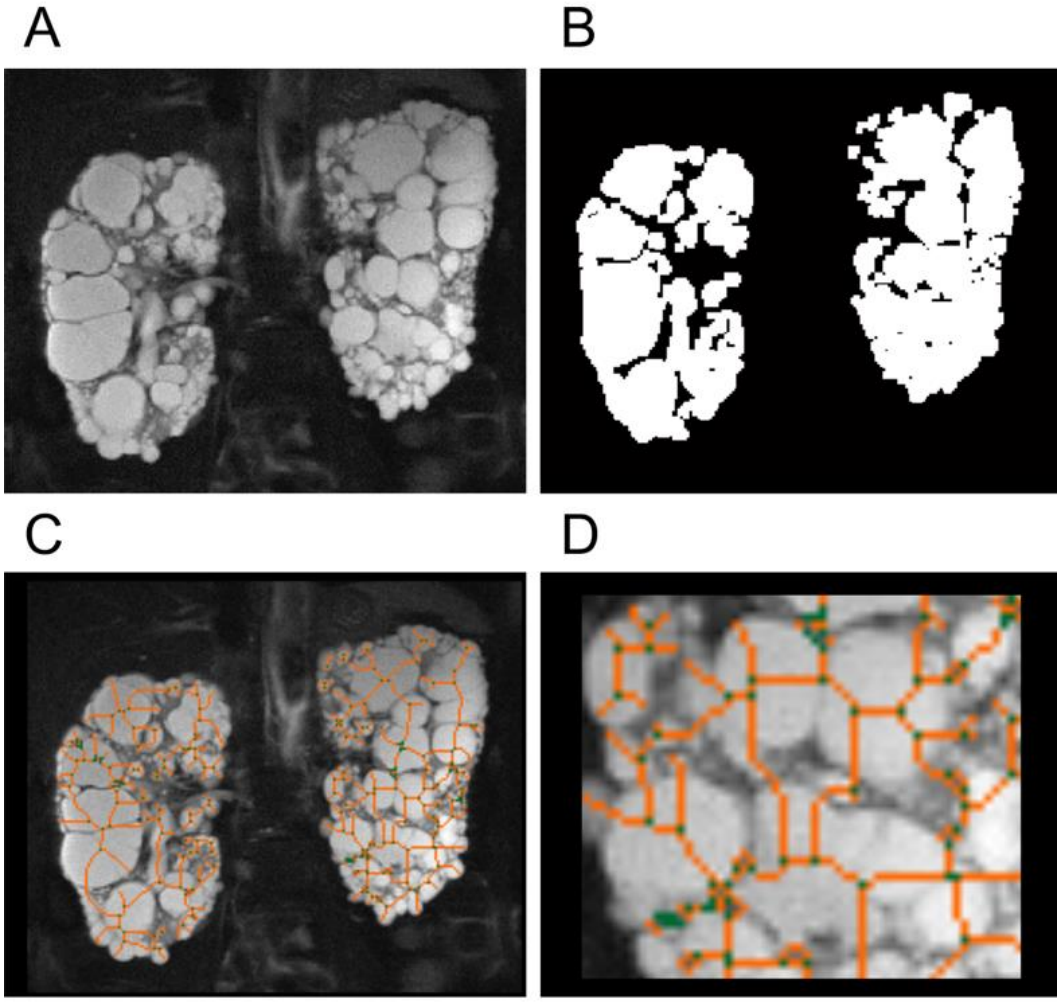

Figure 3. The cyst-like geometric models of uniform size and different numbers of circles with extracted skeletons

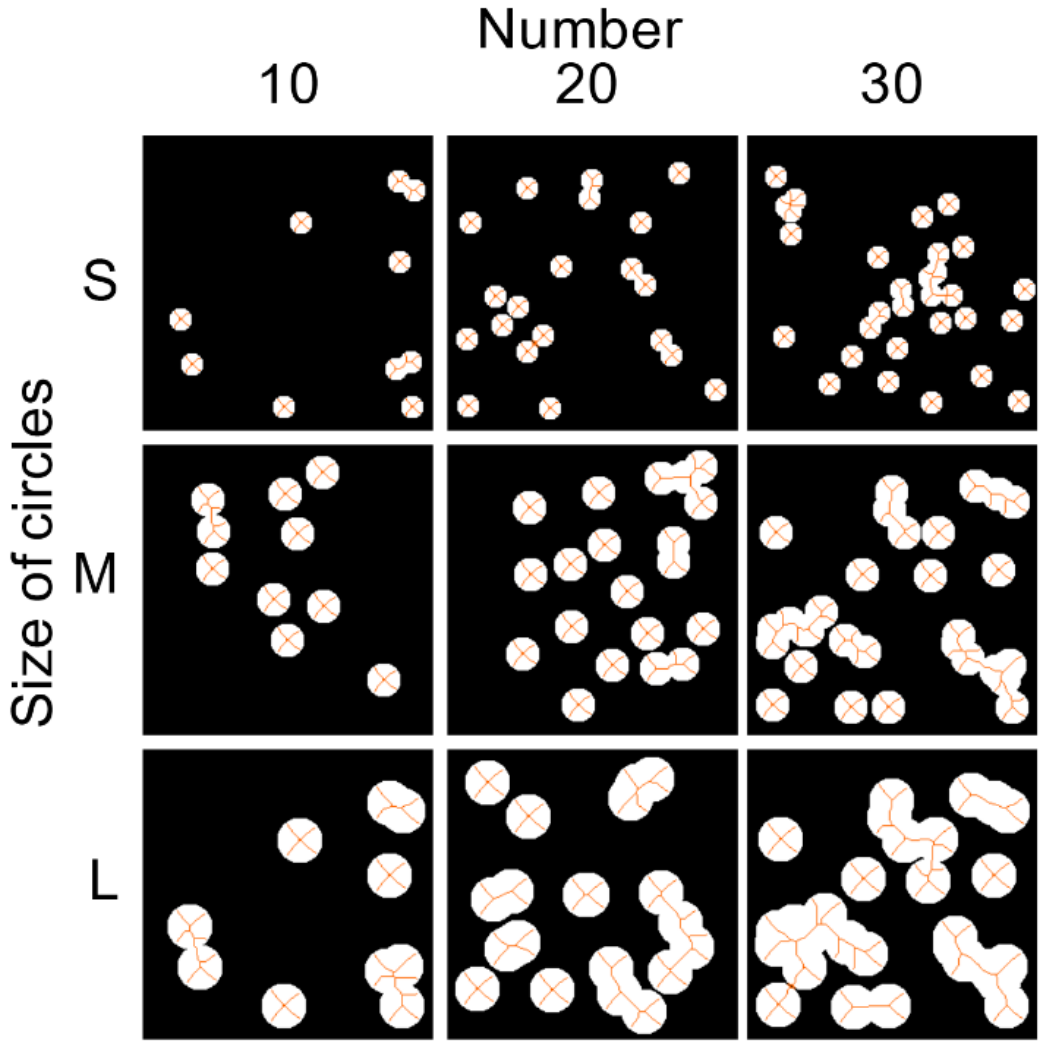

Figure 4. The cyst-like geometric models consist of 30 various sized circles with extracted skeletons

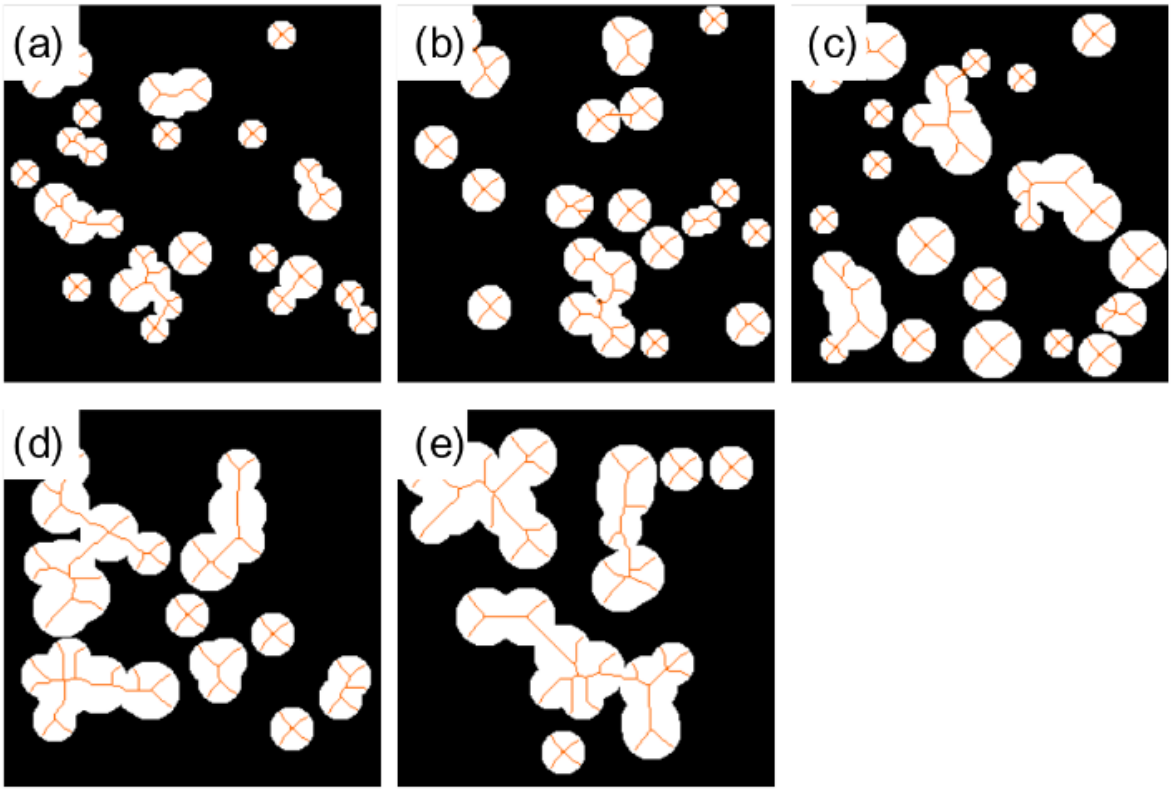

Figure 5. Relationship between number of circles and number of branches
Radius of circles: S 10 pixels, M 20 pixels, L 30 pixels, and LL 40 pixels

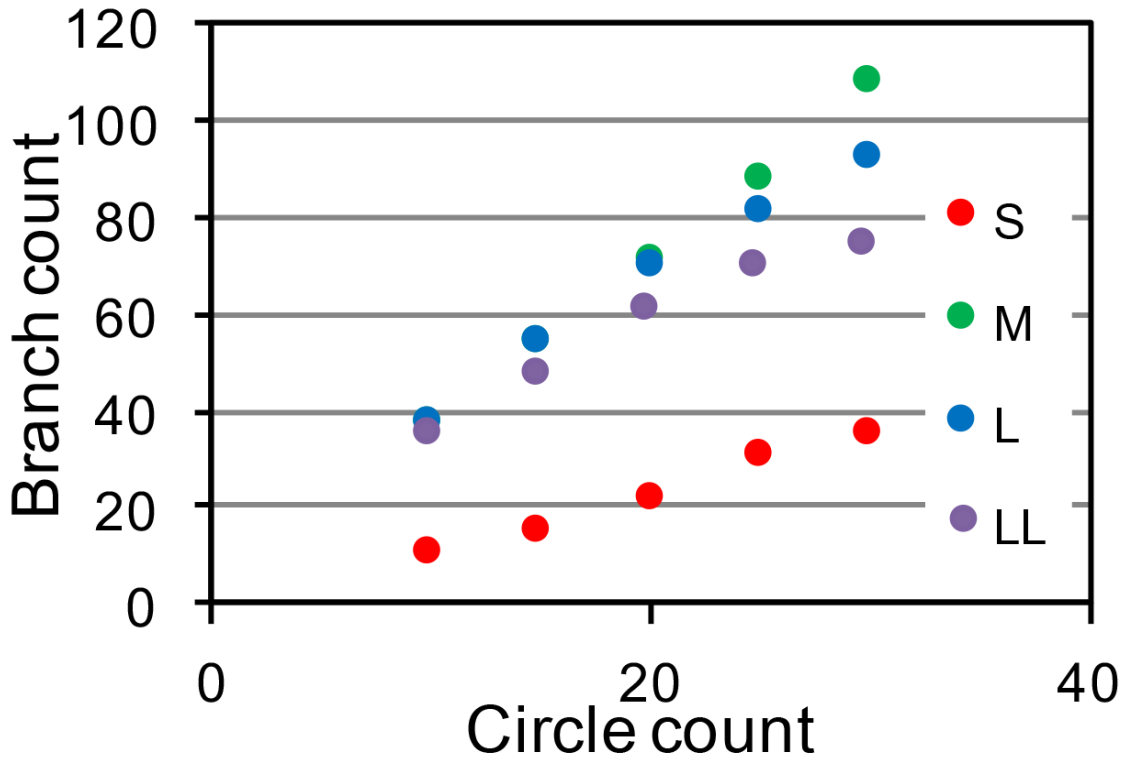

Figure 6. The cumulative probability curves of the branch length processed from Fig.4.

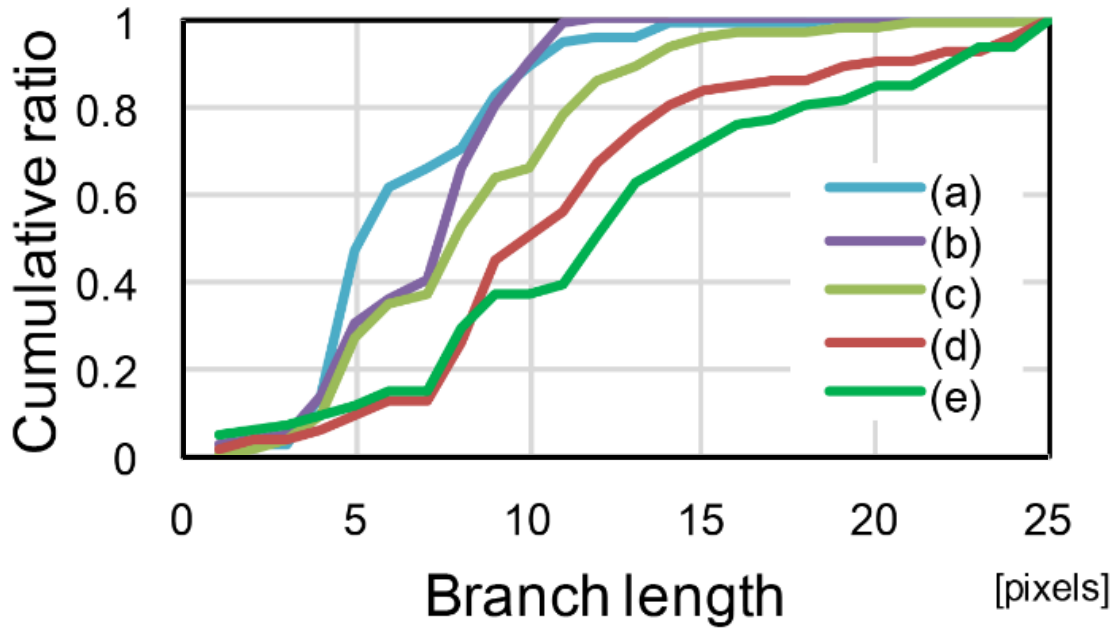

Figure 7. Relationship between the total cyst area measured manually and by the proposed method and the reference value (correlation coefficient 0.97, $p<0.01$)

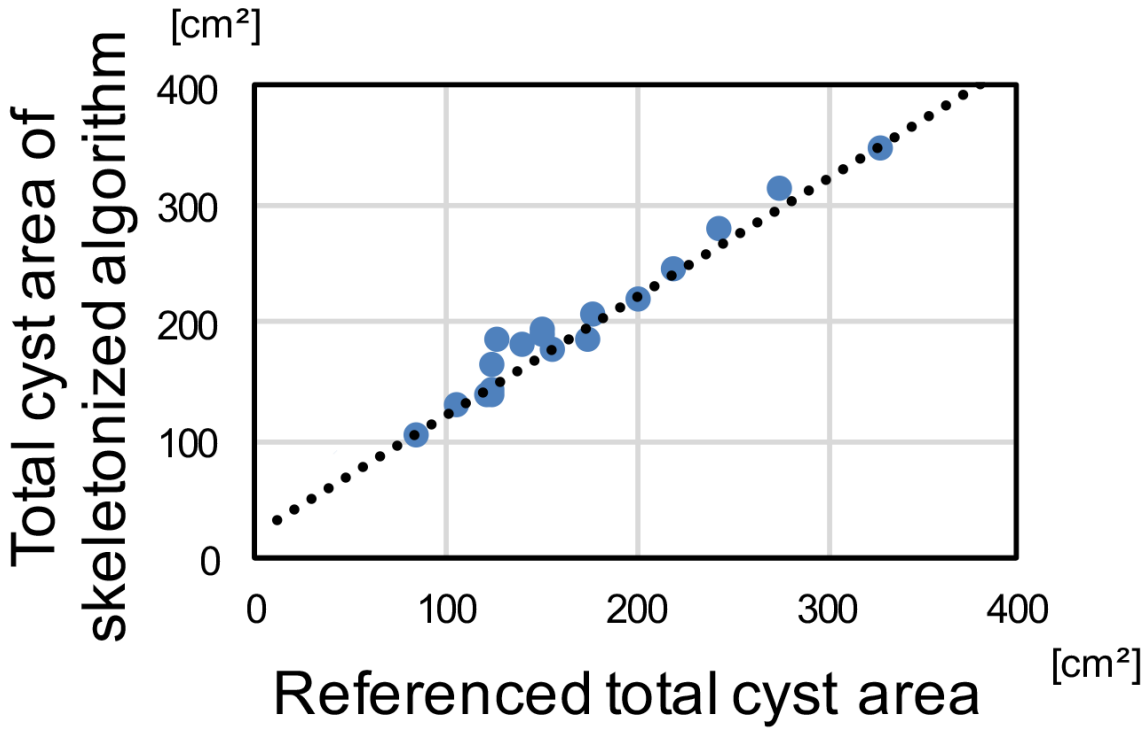

Figure 8. Relationship between number of cyst and number of branches

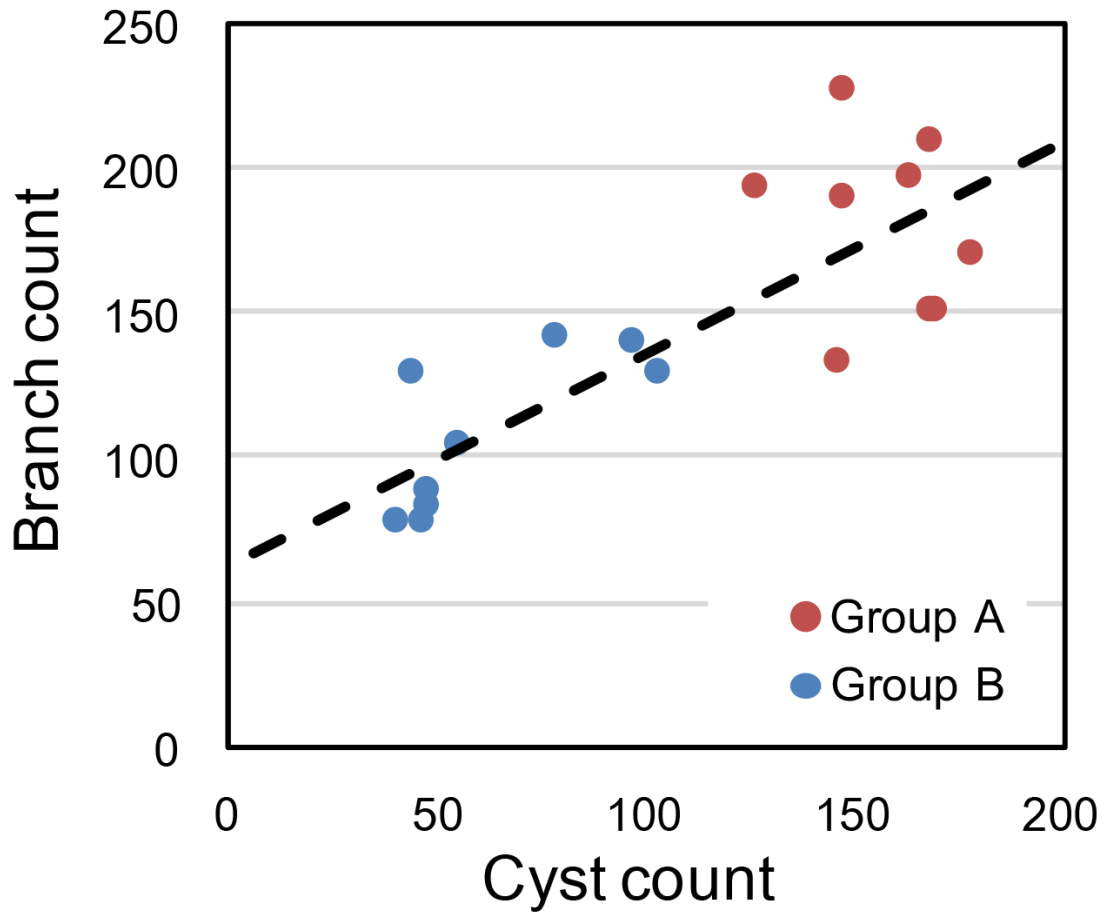

Figure 9. Differences of skeletonization results by morphological characteristics of renal cysts in MR images. Group A is the images in which the number of cyst was more than the average and Group B includes the other images.

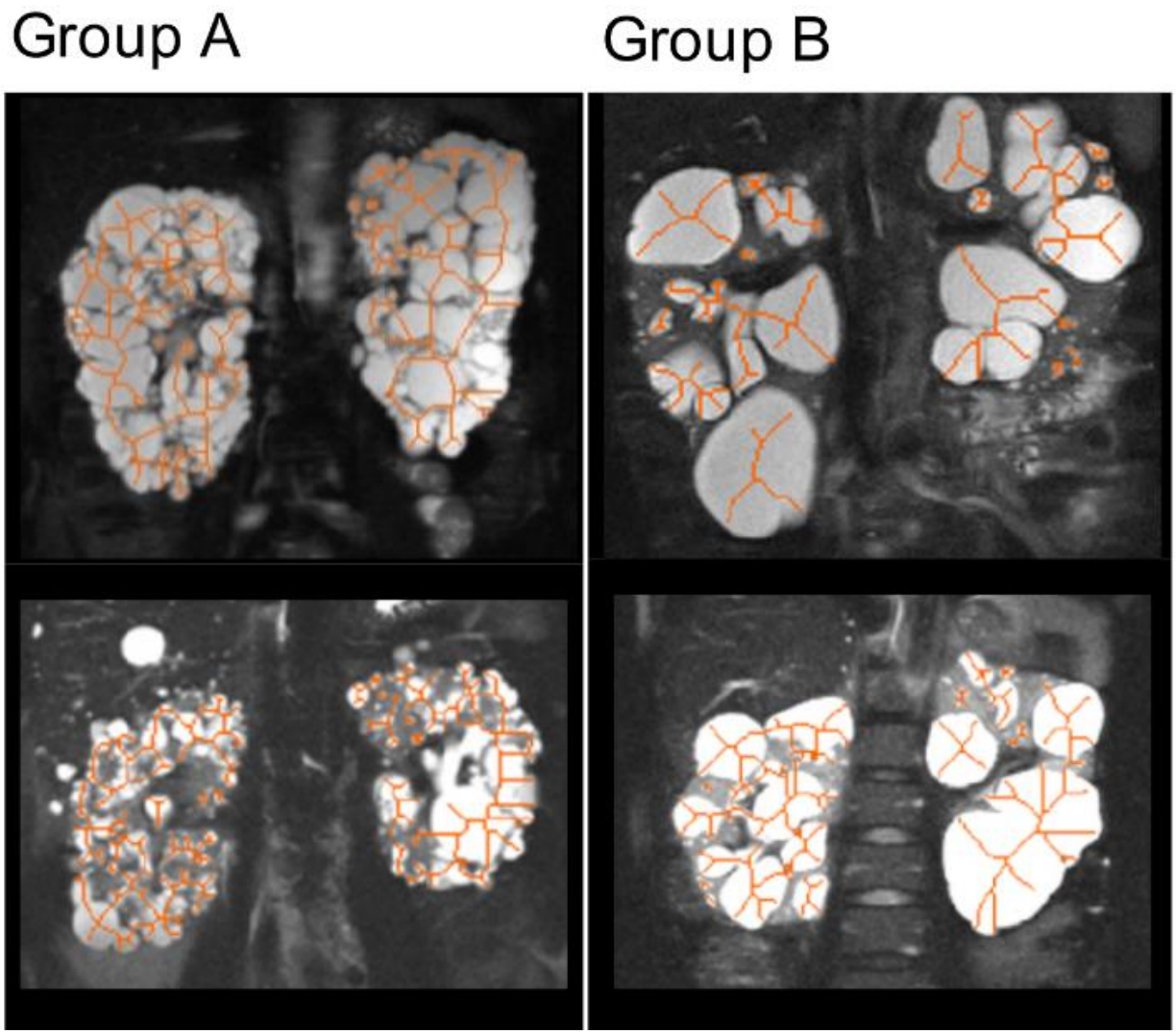

Figure 10. Distribution pattern of cysts in the four samples in Fig.8 using results of (A) manual counting and (B) skeletonization. Red and blue lines correspond to Group A and B in Fig.8, respectively.

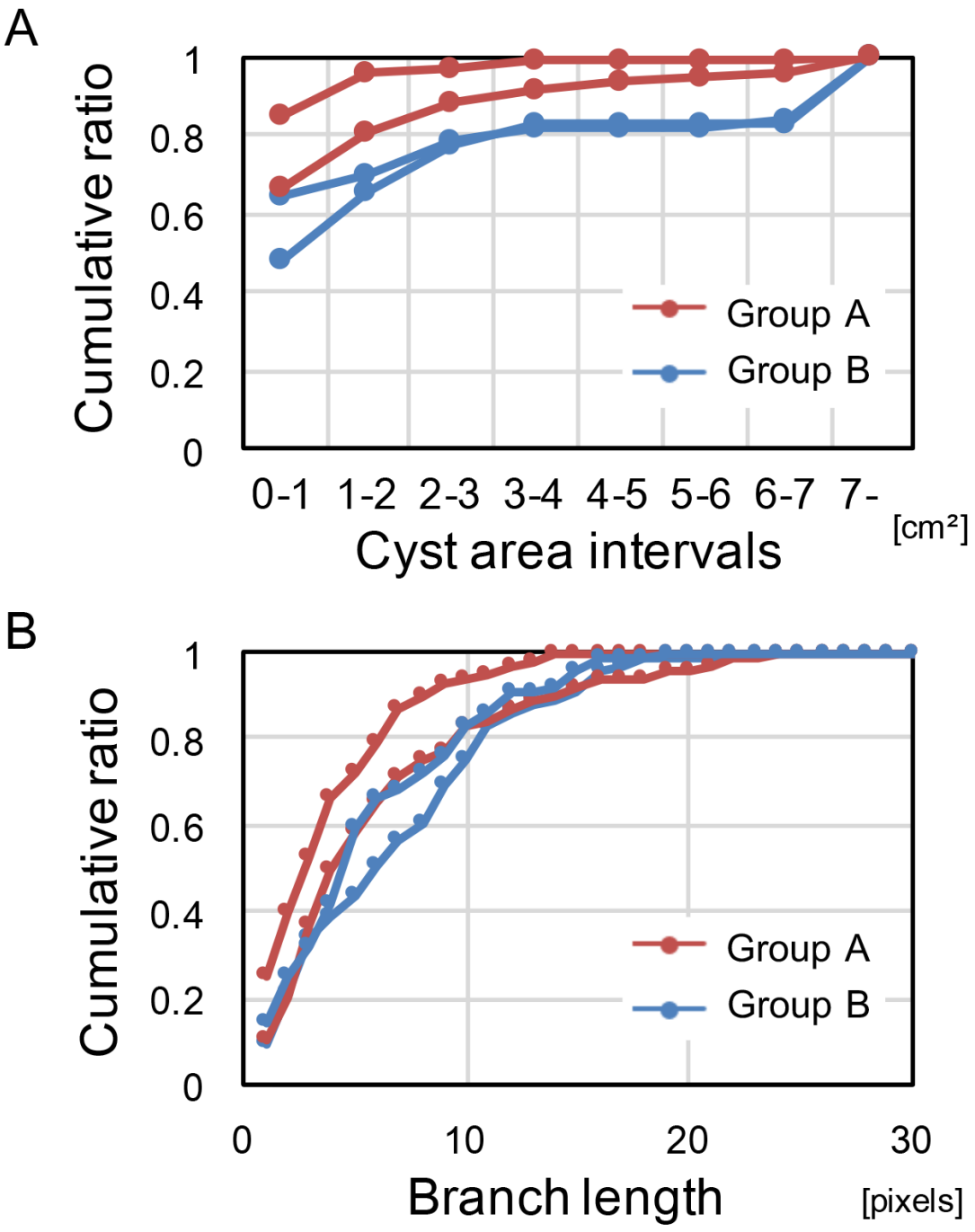

Figure 11. Difference in the average distribution pattern of cysts in all 18 samples in (A) manual counting and (B) skeletonization. Color of lines corresponds to Fig. 9.

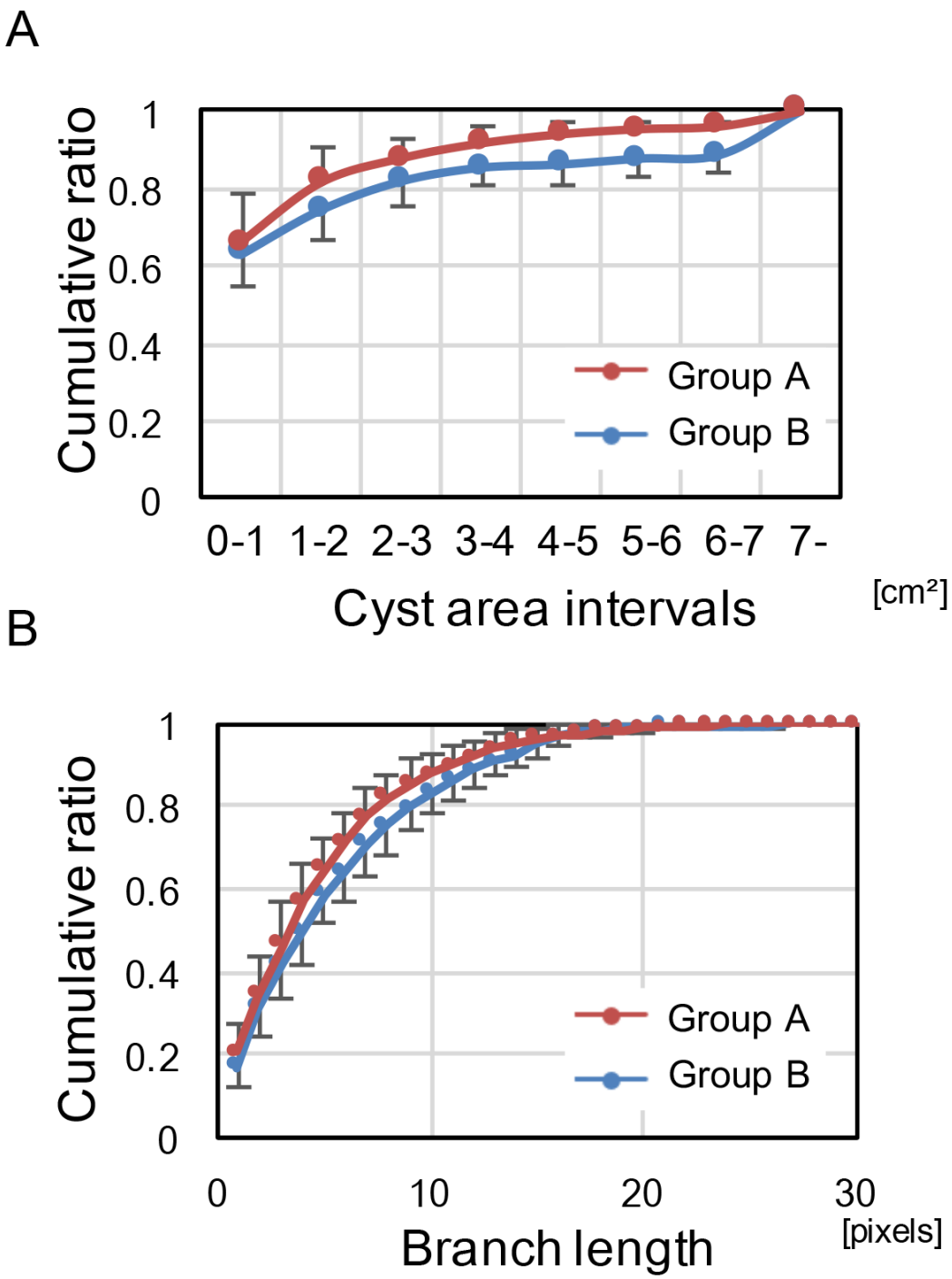

Table 1. Statistical comparison between the separated groups of number of cyst and branches and AUC of cyst area and branch length.

	Counted or Extracted #		AUC of CDF	
	Cysts (reference)	Branches	Cyst area (reference)	Branch length
Group A	157.3±15.6	179.9±29.1	7.13±0.35	25.82±0.99
Group B	66.3±22.8	106.1±25.4	6.68±0.39	25.14±0.85
p	<0.01	<0.01	<0.05	0.08

Welch's *t*-test

Journal of Medical Imaging and Health Informatics
平成29年1月　印刷中